

An EIS study on the capacity fades in $\text{MmNi}_{3.6}\text{Al}_{0.4}\text{Mn}_{0.3}\text{Co}_{0.7}$ metal-hydride electrodes

M. Raju*, K. Manimaran, M.V. Ananth, N.G. Renganathan

Central Electrochemical Research Institute, Karaikudi 630 006, India

Received 16 July 2006; received in revised form 19 September 2006; accepted 19 September 2006

Available online 9 November 2006

Abstract

Capacity fade, generally observed in metal-hydride electrodes of nickel metal-hydride batteries with prolonged cycling, is a problem of concern. To investigate the capacity fade, electrochemical impedance spectroscopy (EIS) measurements were performed in lanthanum rich mischmetal alloy ($\text{MmNi}_{3.6}\text{Al}_{0.4}\text{Mn}_{0.3}\text{Co}_{0.7}$) electrodes. The impedance measurements were conducted during charging at different stages of cycle life. A novel approach was made to get reaction resistances and limiting currents from impedance data based on an equivalent circuit for finite spherical hydrogen diffusion. The main cause of the capacity fade occurring in metal-hydride electrodes with number of cycles was due to particle pulverization and consequent poor hydrogen desorption kinetics, thereby making it more difficult for hydrogenation to occur because of passivation and resistance of electron conduction between the alloy particles.

© 2006 International Association for Hydrogen Energy. Published by Elsevier Ltd. All rights reserved.

Keywords: Hydrogen storage alloys; Ni/MH batteries; Cyclic stability; Impedance measurements; Electrochemical kinetics

1. Introduction

Of late, nickel metal-hydride batteries find wide applications in consumer electronics and electric vehicles since they have high energy density, long cycle life and environmentally benign when compared to conventional nickel cadmium batteries. Variety of hydrogen storage alloys have been used as active material for negative electrodes in nickel metal-hydride batteries. Extensive work has been done on the Zr–V–Ti and LaNi_5 -based alloys (AB_2 and AB_5) [1–4] due to their high hydrogen storage capacity. However, the primary limiting factor for developing a practical metal-hydride battery is the severe capacity decay of the negative alloy electrodes upon cycling. One of the main causes of the capacity losses of the negative electrode is pulverization and disintegration of the alloy during repeated charge–discharge cycling. The specific surface area of LaNi_5 alloy increases due to pulverization and the formation of new active sites during charge/discharge cycling.

The capacity of the LaNi_5 based alloy decreases [5] drastically due to increase in contact resistance of alloy particles which is influenced by pulverization and thereby decreasing the charge efficiency. The oxidation of alloy is accelerated through continuous pulverization [6–8] and contributes to severe capacity fade upon cycling. Despite some publications on the subject, the concept of capacity fade is not yet thoroughly understood.

Electrochemical impedance is a powerful tool for characterization of metal-hydride electrodes, and has been widely used [9,10]. Also, development of mathematical models is often required in order to elucidate the contributions from the various processes to the measured impedance [11]. An overview of mathematical models describing impedance response related to various chemical/electrochemical reaction as well as transport phenomena is given by Lasia [12]. For metal hydrides, some studies have focused on determination of the hydrogen diffusion coefficient, mainly by fitting of data to modified Warburg impedance [13,14]. A physical impedance model has previously been developed by Valøen et al. [15], including a discrete particle size distribution, and finite resistivity of the solution in the pores by inclusion of a de Levie pore resistance. An impedance model based on porous electrode theory, including a discretized

* Corresponding author. Tel.: +91 4565 227555; fax: +91 4565 227713.
E-mail address: mraju@gmail.com (M. Raju).

Nomenclature

a_{OH^-}	activity of OH^- in solution, mol cm^{-3}	K_1	equilibrium constant of charge-transfer reaction
$a_{\text{H}_2\text{O}}$	activity of H_2O in solution, mol cm^{-3}	N_m	available concentration of adsorbed hydrogen, mol cm^{-3}
C_{dl}	double layer capacitance, F cm^{-2}		
C_d	capacitance associated with hydrogen diffusion, F cm^{-2}		<i>Greek symbols</i>
C_{ht}	absorption capacitance, F cm^{-2}	φ_0	equilibrium potential of hydride electrode, V
D_α	Diffusion coefficient of hydrogen in the α phase of metal-hydride particles, $\text{cm}^2 \text{s}^{-1}$	Γ	maximum coverage degree of adsorbed hydrogen on the electrode surface, mol cm^{-3}
F	Faraday's constant, 96487 C mol^{-1}	σ	impedance coefficient of hydrogen diffusion
k_1 and k_{-1}	forward and backward rate constants of charge-transfer reaction, respectively, cm s^{-1}		

particle size distribution was developed by Lundqvist and Lindbergh [16].

In the present study, an attempt is made to calculate the limiting currents from electrochemical impedance spectroscopy (EIS) data for understanding the capacity fade during life cycling.

2. Experimental

The hydrogen storage alloy $\text{MmNi}_{3.6}\text{Al}_{0.4}\text{Mn}_{0.3}\text{Co}_{0.7}$ (Treibacher, Austria) having particle size of $75 \mu\text{m}$ was used for electrode preparation and analysis. The crystal structure was identified by X-ray diffractogram. The metal-hydride electrodes were prepared by mixing the alloy powder with a conducting material and a binder. The mixture was pasted onto either sides of nickel foam substrate and then, it was pressed under 1000 kg cm^{-2} . The pressed electrode was heated to 398°K in a reducing atmosphere. The electrochemical impedance measurements of the metal-hydride electrodes were performed in a three-electrode test cell using Autolab PGSTAT30 potentiostat–galvanostat. The reference electrode was Hg/HgO electrode filled with 6M KOH solution and the counter electrode was sintered nickel hydroxide electrode. The impedance measurements were carried out initially for as-assembled electrode, and then, the experiments were performed after charging at 300 mA g^{-1} for 7 h. Further the MH electrode was discharged at 250 mA up to -0.65 V . The procedure was repeated after 12th, 60th and 120th charge cycles. LCN Bitrode Model 2-10-12 cycle life tester was used for galvanostatic charge/discharge cycling. The morphology of the as-assembled alloy electrode and its changes due to pulverization after 120th charge cycle were analyzed by SEM figures using Hitachi Model: S-3000H microscope.

3. Approach

The aim of our present study is to get reaction resistances and limiting currents from impedance data. Usually limiting currents are obtained experimentally through Tafel polarization. It is known that for a metal-hydride electrode with a flat pressure plateau at a low state of discharge (SOD),

the resistance measured from linear micro polarization is approximately equal to the sum of three resistances measured from AC impedance, namely, charge-transfer, hydrogen-transfer and hydrogen-diffusion resistances; however, when the SOD is high, the resistance measured from linear micro polarization is higher than total resistances measured from AC impedance [17]. The methodology is as follows.

According to the mathematical model developed by Wang et al. [17], the resistance parameters of a metal-hydride alloy electrode, R_s , R_{ct} , R_{ht} could be calculated from the EIS by constructing the equivalent circuit, where R_s is the solution resistance, R_{ct} is the charge-transfer resistance and R_{ht} is hydrogen-transfer resistance. For a metal-hydride electrode with a flat pressure (potential) plateau, diffusion impedance (Z_d) can be simplified as a Warburg impedance. Z_d is in series with a capacitance in the high frequency range. At low frequencies, Z_d can be defined as the resistance (R_d) in parallel with a resistance (R) and a capacitance (C_d) in series. The total resistance measured from AC impedance is

$$R_{\text{total}} = R_{\text{ct}} + R_{\text{ht}} + R_d. \quad (1)$$

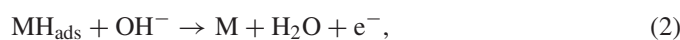
The above resistance can be calculated using the limiting currents of the various processes taking place. Computations of various resistances from the impedance diagrams were made by fitting using the equivalent circuit. Diffusion impedance was further decomposed to get resistance (R_d) and capacitance (C_d) for hydrogen diffusion into the bulk of the alloy from the low frequency data.

From the various values of resistances obtained from impedance data in the above equations the various limiting currents are calculated and the rate constant of the process are also calculated.

Exchange current density and equilibrium constant for the metal-hydride electrode have been determined as suggested by Wang et al. [17]. The Diffusion coefficient values have been determined as reported elsewhere [14].

The anodic polarization involves a charge-transfer process followed by the hydrogen transition from the adsorbed site in the near surface to the adsorbed site on the electrode surface and then the diffusion of adsorbed hydrogen from the bulk to the near surface.

The above process can be represented as follows:



wherein the phase transitions from MH to β phase and from MH to α phase are not considered. Hydrogen absorption from bulk to surface was calculated from the impedance plots.

4. Results and discussion

The crystallographic structure of the alloy $\text{MmNi}_{3.6}\text{Al}_{0.4}\text{Mn}_{0.3}\text{Co}_{0.7}$ was analyzed by the X-ray diffractogram and the pattern is given in Fig. 1. The observed diffraction lines correspond to the JCPDS card no. 25-1136. The alloy has CaCu₅-type hexagonal structure and its lattice parameters a and c are 5.0027 and 4.0558 Å, respectively. The unit cell volume is 87.90 Å³.

The discharge performance of MH electrode is shown in Fig. 2. After the activation cycles, the cell delivered a constant performance up to 50 cycles, at C₅ rate. A slight capacity fade was observed after 60 cycles and it continued up to 120 cycles. The Nyquist plots for the electrode without charging and at the end of 1st charge, 12th charge, 60th charge and 120th charge cycles, respectively, consists of two semicircles, Fig. 3a–e. The semicircle in the high frequency region is attributed to the contact resistance between the alloy particle and the current collector. The other semicircle is attributed to a charge-transfer process on the electrode surface. The interception at high-frequency region is directly related to electrolyte resistance. This is in agreement with the literature [18]. The semicircles obtained reveal a clear monotonic decrease in resistance up to 60th cycle and thereafter it increases with increase in loss of contact between particles due to pulverization. The semicircles can be correlated with the electrical double layer and the charge-transfer resistance.

Fig. 3a shows the Nyquist plot of the as-assembled electrode (before 1st charging), which indicates high resistance.

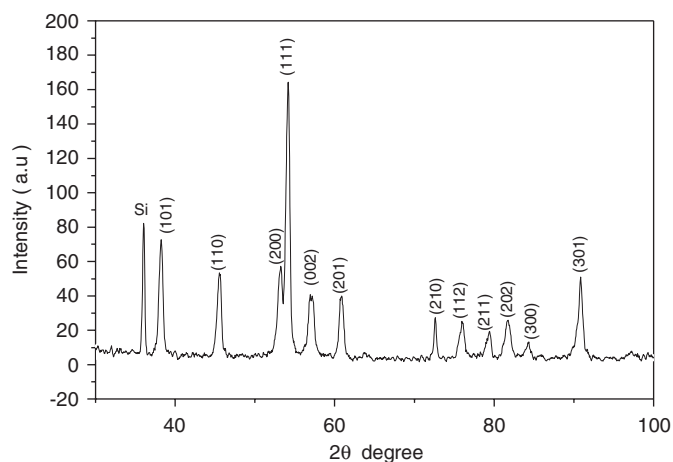


Fig. 1. XRD pattern of $\text{MmNi}_{3.6}\text{Al}_{0.4}\text{Mn}_{0.3}\text{Co}_{0.7}$ metal-hydride alloy.

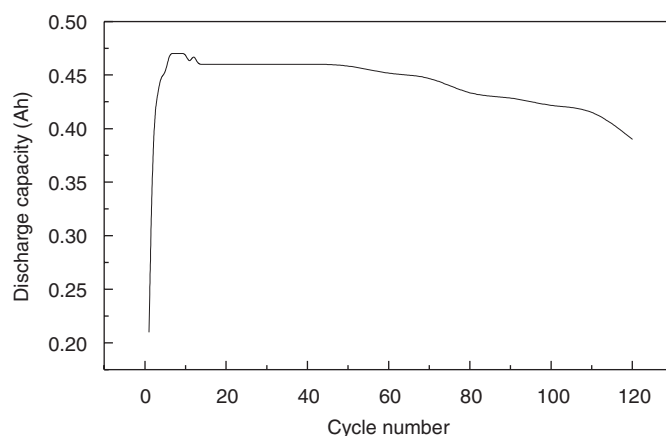


Fig. 2. Discharge performance of $\text{MmNi}_{3.6}\text{Al}_{0.4}\text{Mn}_{0.3}\text{Co}_{0.7}$ metal-hydride electrode.

Fig. 3b–d represents the variation of resistances at the end of charging at 1st, 12th and 60th cycles, respectively. The resistance decreases gradually from 1st charging to 60th charging thereby indicating the stability in discharge capacity as reflected in cycle life performance. Fig. 3e indicates the behavior of the alloy electrode at the end of 120th charge cycle, the resistance increases compared to 60th charge cycle indicative of occurrence of capacity fading. Thus with progressive cycling, only negligible changes occur in the smaller semicircle in the high frequency region, representing the contact resistance between the alloy particles and the current collector. But the larger semicircle in the low-frequency region (defined as a charge-transfer resistance for hydrogenation reaction) is changed, that is, the radius of the larger semicircle in the low-frequency region is decreased first and then increased with cycling, which indicates that the charge-transfer resistance of the electrode surface is decreased first and then increased. Electrolyte resistance is found to initially decrease up to 12th cycle and increase thereafter, where the increase of contact area between electrolyte and electrode lowers the electrolyte resistance.

The understanding of variation in resistance at the end of charge will be the main focus of the present investigation. With the help of equivalent circuits [17] the various components of resistances are calculated from the experimental impedance plots.

From the values of charge-transfer resistance, expressed for a geometric surface area of the electrode, the results are analyzed in detail. It is known that the increase in charge-transfer resistance deteriorates the electrochemical performance of the alloy electrodes. It has been suggested that an oxide/hydroxide film is formed and grows on the surface, which reduces the electrochemical catalytic activity of the electrode surface and has a detrimental effect on the electrochemical hydrogen reaction of the alloy and thus lowers the discharge capacity [19]. As expected, the charge-transfer resistance is very high at 2828 Ωcm² for as-assembled electrode. The value drastically falls after 1st charging and decreases gradually thereafter up to 60 cycles and marginally increases after that. This explains the onset of capacity fade observed in cycle life experiments.

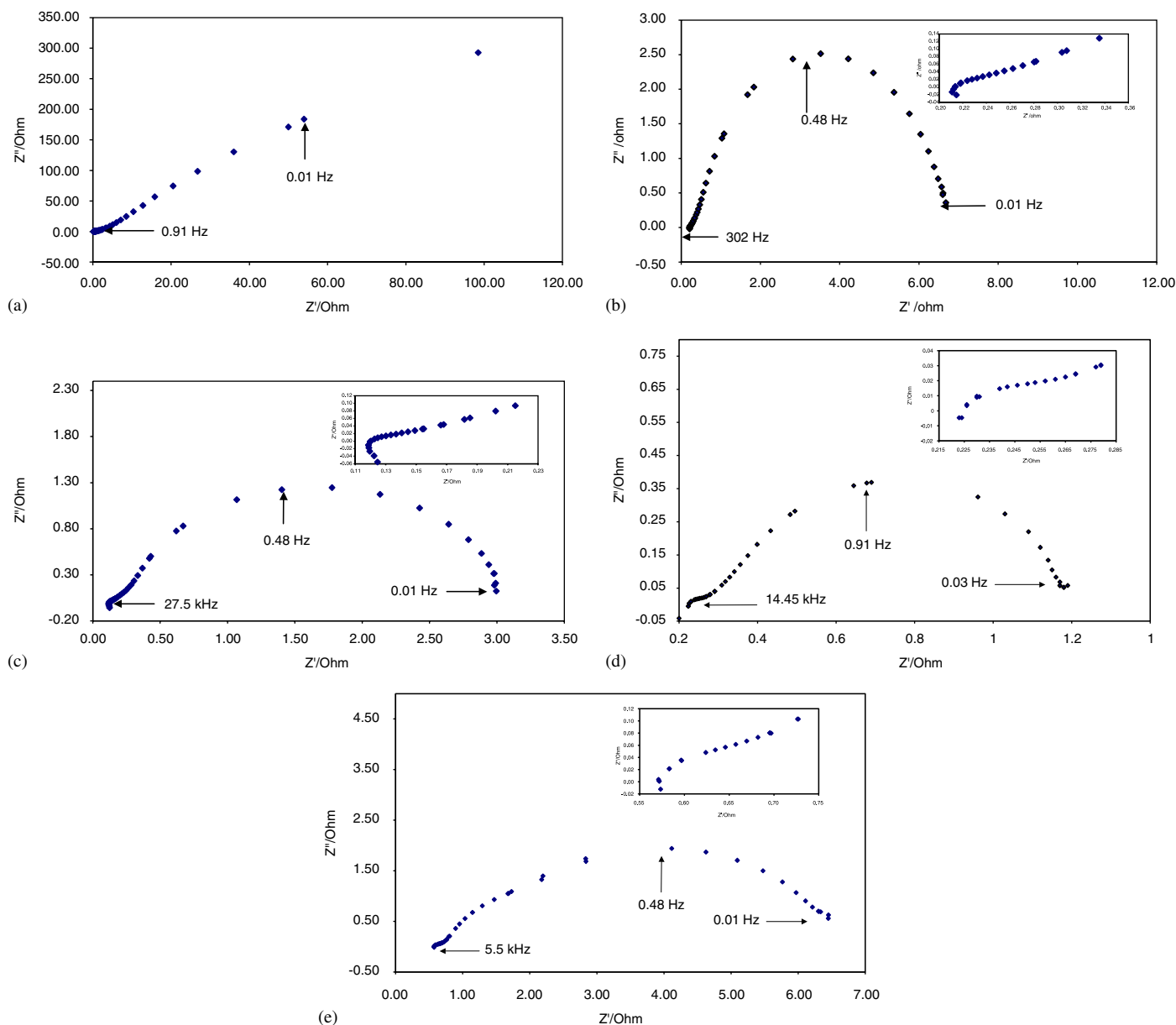


Fig. 3. (a) Nyquist plot of $\text{MmNi}_{3.6}\text{Al}_{0.4}\text{Mn}_{0.3}\text{Co}_{0.7}$ metal-hydride electrode (as-assembled). (b) Nyquist plot of $\text{MmNi}_{3.6}\text{Al}_{0.4}\text{Mn}_{0.3}\text{Co}_{0.7}$ metal-hydride electrode (after 1st charging). (c) Nyquist plot of $\text{MmNi}_{3.6}\text{Al}_{0.4}\text{Mn}_{0.3}\text{Co}_{0.7}$ metal-hydride electrode (after 12th charging). (d) Nyquist plot of $\text{MmNi}_{3.6}\text{Al}_{0.4}\text{Mn}_{0.3}\text{Co}_{0.7}$ metal-hydride electrode (after 60th charging). (e) Nyquist plot of $\text{MmNi}_{3.6}\text{Al}_{0.4}\text{Mn}_{0.3}\text{Co}_{0.7}$ metal-hydride electrode (after 120th charging).

Thus, it is obvious that, with cycling, the R_{ct} values decrease initially from $473 \text{ m}\Omega \text{ cm}^2$ (1st cycle) to $2.085 \text{ m}\Omega \text{ cm}^2$ (60th cycle) and then increase to $177.6 \text{ m}\Omega \text{ cm}^2$ (120th cycle). It suggests that the reaction of hydrogen at the surface of alloy electrode changes more easily up to 60 cycles, which can be attributed to the presence of a surface with high electrocatalytic activity. And then, with further cycling, the reaction of hydrogen at the surface tends to become difficult, which may be the result of formation and increase of hydroxide film at the alloy surface causing a surface passivity [20].

The exchange current density I_0 is a powerful parameter for measuring the kinetics of the electrochemical hydrogen reaction [21,22]. The electrode with higher exchange current density

and limiting current density has increased high-rate dischargeability [23]. Exchange current density (I_0) increases steadily from 24.7 to 3719 mA g^{-1} up to 60th charging and it reduces to a low value of about 1100 mA g^{-1} at 120th charging, which again indicates capacity fade as hydrogen exchange is becoming difficult after 60 cycles. The diffusion coefficient values however follow a different trend. Only slight variations could be seen. This implies that the diffusion of hydrogen in the alloy is similar due to the same bulk properties and the difference between them is only in the surface state.

Table 1 represents the values of reaction resistances and limiting currents calculated based on the models described from parameters obtained based on impedance data at the end of 1st,

Table 1
Kinetic parameters of the electrode

Parameters	1st charging	12th charging	60th charging	120th charging
R_s , $m\Omega\text{cm}^2$	236.4	130.1	237.1	588
C_{dl} , pF	10.28	21.3×10^9	1.0	0.860×10^9
R_{ct} , $m\Omega\text{cm}^2$	473	204.8	2.085	177.6
C_{ht} , mF	43.0	128.1	24.98	13.36
R_{ht} , Ωcm^2	12.95	11.49	6.15	12.89
R_d , Ωcm^2	7.45	8.9	5.24	7.42
C_d , pF	1.0	1.0	4.73×10^9	22.58×10^9
I_0 , mA g^{-1}	24.7	54	3719	1100
D , m^2S^{-1}	0.9642×10^{-9}	0.133×10^{-8}	0.8794×10^{-9}	1.837×10^{-7}
A	1.13	1.13	1.13	1.13
I_{Lbd} , A cm^{-2}	6.873×10^{-3}	5.75×10^{-3}	9.77×10^{-3}	6.9×10^{-3}
I_{Lbs} , A cm^{-2}	6.49×10^{-3}	2.457×10^{-5}	2.355×10^{-3}	2.099×10^{-4}
I_{Ldb} , A cm^{-2}	5.0×10^{-3}	2.495×10^{-3}	3.38×10^{-8}	4.968×10^{-9}
I_{Lsb} , A cm^{-2}	0.253	0.186	4.527×10^{-4}	4.86×10^{-4}
K_1	1.650	1.650	1.650	1.650

12th, 60th and 120th charge cycles, respectively. The variation of limiting current density, I_L , will be generally concordant with that of I_0 . The limiting current density is mainly controlled by the hydrogen diffusion in the bulk of alloys [24]. The larger the limiting current density I_L , the higher is the rate of the hydrogen diffusion inside the alloy. In our analysis, the hydrogen limiting currents, surface to bulk decreases rapidly and this explains the reason for capacity fade. Whereas, comparatively no significant variations in limiting currents of hydrogen diffusion from bulk to surface could be seen, the limiting current of hydrogen diffusion from the surface to bulk decreases from a large value to a lower value as number of charge cycles proceeds. All this is due to particle pulverization of hydrogen diffusion from bulk to surface. It can be better understood from the increase in solution resistance as charge cycle progresses.

An in-depth analysis of limiting current values indicates that the limiting current of hydrogen diffusion from the bulk to the surface of particle (I_{Lbs}) shows a decline in the initial stages from 6.49×10^{-3} to $2.457 \times 10^{-5} \text{ A cm}^{-2}$ up to 12 cycles followed by increase to about $2.355 \times 10^{-3} \text{ A cm}^{-2}$ up to 60 cycles and marginal decline to about $2.099 \times 10^{-4} \text{ A cm}^{-2}$ thereafter. I_{Lsb} —limiting current of hydrogen diffusion from the surface to the bulk of particle, shows a progressive decline from 0.253 A cm^{-2} , which intensifies to $4.86 \times 10^{-3} \text{ A cm}^{-2}$ with cycling. This is indicative of the passivity of the surface and increase in contact resistance at the surface. I_{Lbd} —limiting current of hydrogen transfer from absorbed state to adsorbed state show a wavy pattern (minimum $5.75 \times 10^{-3} \text{ A cm}^{-2}$ and maximum $9.77 \times 10^{-3} \text{ A cm}^{-2}$) within a narrow range. The limiting current of hydrogen transfer from adsorbed state to absorbed state I_{Ldb} shows an intensified decline from $5.0 \times 10^{-3} \text{ A cm}^{-2}$ to as low as $4.968 \times 10^{-9} \text{ A cm}^{-2}$ in the later periods of life cycling. Thus the ease of adsorption to absorption becomes much inferior during cycling. Thus, it is seen that generation of electrochemically inactive surface with cycling is responsible for the observed capacity decay. This is in line with the literature report on commercial Ni-MH cells that

the decrease of discharge capacity is due to an inactive surface that increases the charge-transfer resistance of the battery [25]. Thus, the electrode needs to be modified with appropriate surface structure with minimal particle pulverization. It is reported in the literature that Ni sites on the surface of the metal-hydride electrodes play an important role in hydrogen adsorption [26].

The charge-transfer resistance (R_{ct}) decreases gradually from $473 \text{ m}\Omega\text{cm}^2$ at 1st charging to $2.085 \text{ m}\Omega\text{cm}^2$ at 60th charging and increases thereafter, while double layer capacitance (C_{dl}) shows an irregular trend due to pulverization. But at the end of 120th charge cycle the increased values of R_{ct} and C_{dl} are due to the increase of R_s and C_d . C_d increases considerably after 60th charge cycle. All these accounts for accumulation of charges at the particle interface due to particle pulverization. Hence R_s increases as the inter particle granular resistance increased. So capacity fade is accounted in spite of faster diffusion at 120th charge cycle compared to 12th charge cycle.

Fig. 4a and b present the scanning electron micrographs of $\text{MmNi}_{3.6}\text{Al}_{0.4}\text{Mn}_{0.3}\text{Co}_{0.7}$ metal-hydride alloy and the metal-hydride electrode. From the micrographs it is observed that the alloy powder is a heterogeneous mixture of particles with crystalline characteristics. Fig. 4c shows the SEM image of the MH electrode after 120 cycles. Pulverized alloy particles are identified from the scanning electron micrograph and it leads to increase in particle to particle contact resistance and thereby deterioration in capacity. Fig. 5 shows the Bode plot of the impedance spectrum constructed as per the procedure suggested by Yuan et al. [14]. The knee frequency from the Bode plot has been used to obtain the hydrogen diffusion coefficient.

Fig. 6 shows the typical fitting carried out to obtain the various resistance and capacitance parameters. The experimental and equivalent circuit fit diagram agree mostly except at the low frequency side where it is expected to deviate and this may be due to the porosity of the surface.

It is concluded that cycle stability in the investigated alloy can be improved by adopting approaches like an increase of the

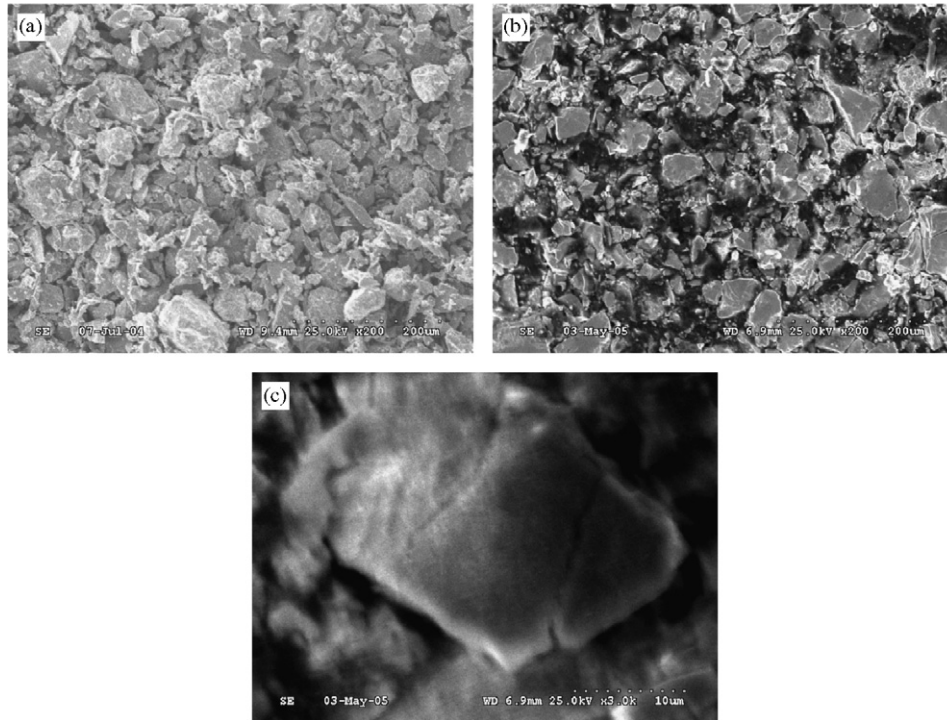


Fig. 4. (a) SEM pictures of $\text{MmNi}_{3.6}\text{Al}_{0.4}\text{Mn}_{0.3}\text{Co}_{0.7}$ metal-hydride alloy. (b) SEM pictures of $\text{MmNi}_{3.6}\text{Al}_{0.4}\text{Mn}_{0.3}\text{Co}_{0.7}$ metal-hydride electrode. (c) SEM pictures of cycled $\text{MmNi}_{3.6}\text{Al}_{0.4}\text{Mn}_{0.3}\text{Co}_{0.7}$ metal-hydride electrode (120th cycle).

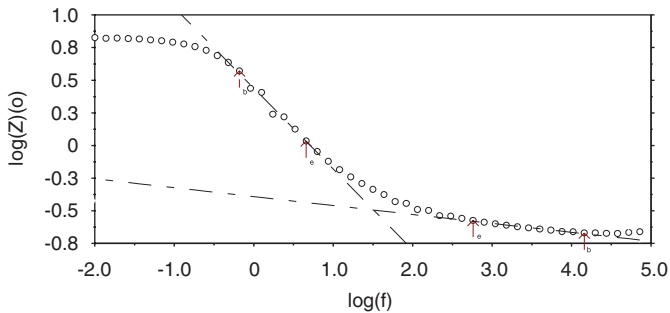


Fig. 5. Bode plot (to obtain the knee frequency at the intersection of two asymptotes).

surface passivity owing to the increase of the oxide coverage on the cycled alloy and a subsequent increase of stability due to the diminution of the exposure of the active material to the alkaline electrolyte [27], or by lowering the Vickers hardness [28], which also may be beneficial for the enhancement of stability over repeated charge/discharge cycles. Also, Ni can form intermetallics which decrease the M–H bond strength to a suitable level [29]. Therefore, tuning the Ni content seems to be a potential method of obtaining a better performance from the alloy.

5. Conclusion

Various resistance parameters and limiting currents of $\text{MmNi}_{3.6}\text{Al}_{0.4}\text{Mn}_{0.3}\text{Co}_{0.7}$ metal-hydride electrode including charge-transfer, hydrogen-transfer and hydrogen diffusion resistances and the limiting currents of hydrogen-transfer from absorbed state to adsorbed state, hydrogen-transfer from adsorbed state to absorbed state, hydrogen diffusion from bulk to the particle surface and hydrogen diffusion from particle surface to bulk are calculated from the impedance plot. Diffusion coefficient and exchange current density are also calculated using the above resistances and currents. Using the derived parameters we could arrive at a method to predict the capacity fade at various charge cycles. Limiting current values obtained, have indicated the main causes of the capacity fade of the negative electrode as pulverization and poor kinetics.

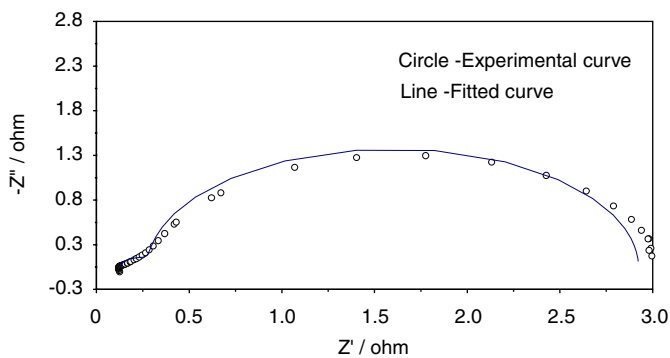


Fig. 6. Typical fitted curve (12th charging).

Acknowledgments

The authors thank the Director, CECRI, Karaikudi for encouragement and permission to publish this work. Thanks are also due to MNES, New Delhi for sanctioning a Grant-In-Aid project on 'Development of Advanced Ni-MH Battery fitted Electric Cycle and Field Studies' in which the above work has been done.

References

- [1] Sui YH, Chen C-P, Wang X-l, Lei Y-Q, Wang Q-D. *J Alloys Compd* 2002;337:214–20.
- [2] Mitrokhin SV, Bezuglaya TN, Verbetsky VN. *J Alloys Compd* 2002;330–332:146–51.
- [3] Du YL, Yang XG, Lei YQ, Zhang MS. *Int J Hydrogen Energy* 2002;27:695–7.
- [4] Simicic MV, Zdujic M, Jelovac DM, Rakin PM. *J Power Sources* 2001;92:250–4.
- [5] Durairajan A, Haran BS, White RE, Popov BN. *J Power Sources* 2000;87:84–91.
- [6] Ye H, Huang Y, Chen J, Zhang H. *J Power Sources* 2002;103:293–9.
- [7] Sakai T, Yoshinaga H, Miyamura H, Kuriyama N, Ishikawa H. *J Alloys Compd* 1992;180:37–54.
- [8] Seo C-Y, Choi S-J, Choi J, Park C-N, Lee PS, Lee J-Y. *J Alloys Compd* 2003;350:324–31.
- [9] Lasia A. In: Conway BE, Bockris JO'M, White RE, editors. *Modern aspects of electrochemistry*, vol. 35. New York; Dordrecht: Academic Plenum Publishers; Kluwer; 2001.
- [10] Johnsen SE, Lindbergh G, Lundqvist A, Tunold R. *J Electrochem Soc* 2003;150:A629–37.
- [11] Svensson AM, Valøen LO, Tunold R. *Electrochim Acta* 2005;50:2647–53.
- [12] Lasia A. In: Conway BE, Bockris JO'M, White RE, editors. *Modern aspects of electrochemistry*, vol. 32. New York; Dordrecht: Academic Plenum Publishers; Kluwer; 1999.
- [13] Haran BS, Popov BN, White RE. *J Power Sources* 1998;75:56–63.
- [14] Yuan X, Xu N. *J Alloys Compd* 2001;329:115–20.
- [15] Valøen LO, Lasia A, Jensen JO, Tunold R. *Electrochim Acta* 2002;47:2871–84.
- [16] Lundqvist A, Lindbergh G. *Electrochim Acta* 1999;44:2523–42.
- [17] Wang C, Soriaga MP, Srinivasan S. *J Power Sources* 2000;85:212–23.
- [18] Hu WK. *J Alloys Compd* 1999;289:299–305.
- [19] Kuriyama N, Sakai T, Miyamura H, Uehara I, Ishikawa H, Iwasaki T. *J Alloys Compd* 1993;202:183–97.
- [20] Yuan AB, Xu NX. *J Alloys Compd* 2001;322:269–75.
- [21] Yayama H, Kuroki K, Hirakawa K, Tomokiyo A. *Jpn J Appl Phys* 1984;23:1619–23.
- [22] Notten PHL, Hokkeling P. *J Electrochem Soc* 1991;138:1877–85.
- [23] Wu M-S, Wu H-R, Wang Y-Y, Wan C-C. *Int J Hydrogen Energy* 2004;29:1263–9.
- [24] Ratnakumar BV, Witham C, Bowman Jr RC, Hightower A, Fultz B. *J Electrochem Soc* 1996;143:2578–84.
- [25] Cheng S, Zhang J, Liu H, Leng Y, Yuan A, Cao C. *J Power Sources* 1998;74:155–7.
- [26] Gao X, Liu J, Ye S, Song D, Zhang Y. *J Alloys Compd* 1997;253–254:515–9.
- [27] Vogt T, Reilly JJ, Johnson JR, Adzic GD, McBreen J. *J Electrochem Soc* 1999;146:15–9.
- [28] Chartouni D, Meli F, Züttel A, Gross K, Schlapbach L. *J Alloys Compd* 1996;241:160–6.
- [29] Kleperis J, Wójcik G, Czerwinski A, Skowronski J, Kopezyk M, Beltowska-Brzezinska M. *J Solid State Electrochem* 2001;5:229–49.